# Supplementary Information

## Colossal magnetocapacitance and scale-invariant dielectric response in phase-separated manganites

Ryan P. Rairigh, Guneeta Singh-Bhalla, Sefaatin Tongay, Tara Dhakal,

Amlan Biswas and Arthur F. Hebard

*Department of Physics, University of Florida, Gainesville, FL 32611-8440*

**Overview**

We report on the use of a trilayer configuration in which the sample under investigation, in our case a 600 Å-thick $(La_{1-y}Pr_y)_{0.67}Ca_{0.33}MnO_3$ (LPCMO) film, comprises the base layer of a metal-insulator-metal (MIM) trilayer capacitor structure (see Fig 1a of Letter). Under certain experimental conditions this unconventional configuration allows for the simultaneous measurement of electrical transport both parallel and perpendicular to the film interfaces. Although the four-terminal Van der Pauw measurement of the LPMCO films provides unambiguous information about transport parallel to the film interfaces, the two-terminal capacitance measurement is more problematic, since it includes contributions from both parallel and perpendicular transport. The following Supplementary section augments our Letter by showing that the two-terminal perpendicular contribution to electronic transport can dominate over the parallel

contribution providing certain experimental constraints are satisfied. When these conditions are satisfied, we show using the well-known Maxwell-Wagner model that the perpendicular contribution is resolved into two series-connected parts: a contribution from the reference AlOx capacitor and a contribution from the intrinsic dielectric response of the LPCMO film. We then show with additional data on films of different thickness how the substrate strain-induced anisotropy, measured by the difference in temperature between the resistance maxima and capacitance minima, decreases and approaches bulk like behavior as the film thickness increases.

**Comparison of longitudinal and perpendicular voltage drops**

The measured voltage of the two-terminal configuration of Fig. 1a of the Letter can have both parallel and perpendicular contributions from currents flowing respectively either along the LPCMO electrode or transverse to the film through the capacitor. Since these contributions cannot be distinguished in a two-terminal measurement, it is necessary when measuring capacitance to establish conditions where the perpendicular voltage drop dominates over the parallel voltage drop. There are two necessary requirements to assure a dominant perpendicular voltage drop: (1) the dc leakage current through the AlOx dielectric is negligible and (2) the measurement frequency is constrained to be within well defined upper and lower bounds determined by sample properties.

We can begin to understand these requirements by modeling the measurement configuration as a resistance $R_s$ in series with the parallel combination of a complex lossy capacitance, $C^*(\omega)= C_1(\omega) - iC_2(\omega)$, and a dc

resistance, $R_0$ (Supplementary Fig. 1a). By lossy capacitance we mean a capacitor that does not pass dc current but does experience loss at ac due to dipole reorientation. Thus the combination of $C^*(\omega)$ shunted by $R_0$ is a leaky

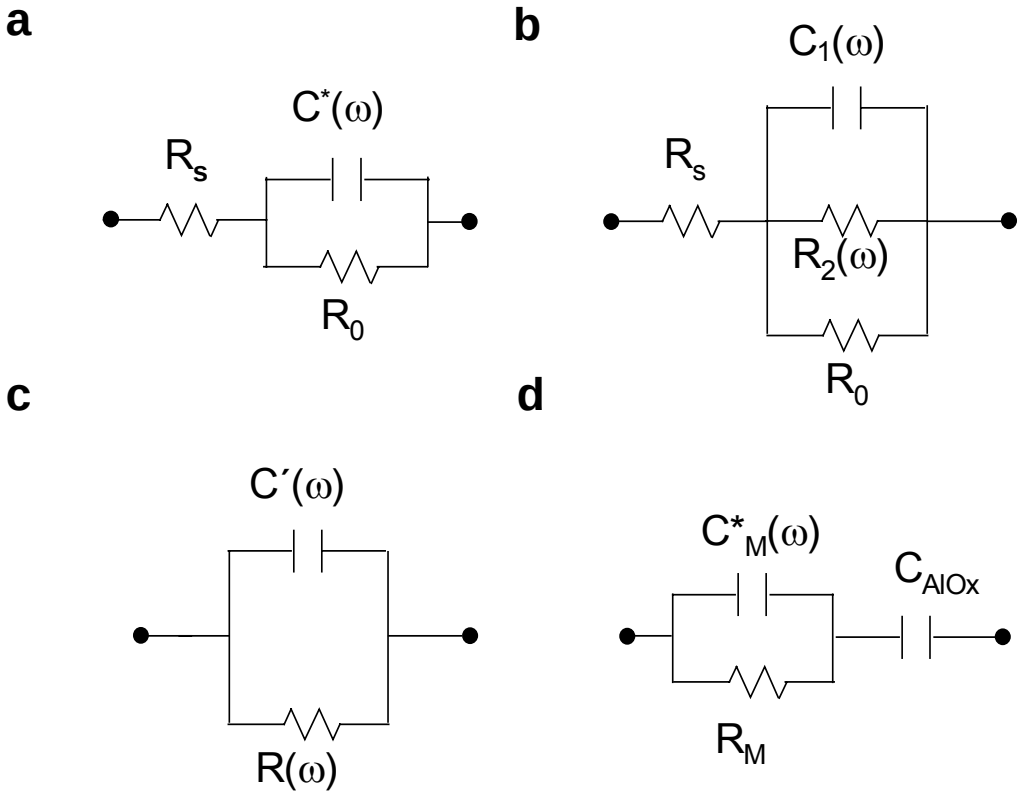


**Supplementary Figure 1 | Circuit diagrams facilitate understanding the sources of longitudinal and perpendicular voltage drops. a,** Circuit equivalent of the two-terminal measurement configuration (Fig. 1a of Letter) where $R_s$ is the series resistance of the LPCMO sample and the parallel combination of a complex (lossy) capacitor $C^*(\omega)$ with a resistor $R_0$ represents the impedance of the LPCMO in series with the aluminum oxide capacitor. In the two-terminal configuration, the longitudinal voltage drop across $R_s$ cannot be distinguished from the perpendicular voltage drop across the parallel combination of $C^*(\omega)$ and $R_0$. **b,** Decomposition of $C^*(\omega) = C_1(\omega) - iC_2(\omega)$ into a parallel combination of $C_1(\omega)$ and $R_2(\omega) = 1/\omega C_2(\omega)$. **c,** Circuit equivalent for the capacitance $C'(\omega)$ and conductance $1/R(\omega)$ reported by the capacitance bridge. **d,** Maxwell-Wagner circuit equivalent for the LPCMO impedance in series with the Al/AlOx capacitor. The LPCMO manganite film impedance is represented as a lossy capacitor $C^*_M(\omega)$ shunted by a resistor $R_M$. There is no shunting resistor across $C_{AlOx}$ because the measured lower bound on $R_0$ is 10 GΩ, well above the highest impedance of the other circuit elements.

capacitor which does pass dc. The resistance $R_s$ includes the parallel resistance $R_{||}$ of the LPCMO and any resistance associated with the LPCMO contact. The negligible resistance of the Al counterelectrode and its associated contact are included in $R_s$. Our measurements at dc establish the conditions $R_0 + R_s > 10^{10}\ \Omega$ (see Methods section of Letter) and $\max\{R_s\} = 10^7\ \Omega$ (Fig. 1b of Letter), which together imply that over the whole range of dc measurements more than 99.9% of the voltage appears across $C^*$. At temperatures away from the resistance peak this figure of merit improves considerably.

Since the capacitance measurements are made at finite frequency, we must consider the more complicated situation of additional current paths and choose conditions to assure that most of the ac potential drop is across $C^*(\omega)$. We do this by redrawing the circuit of Supplementary Fig. 1a to include the ac loss as a resistor $R_2(\omega) = 1/\omega C_2(\omega)$ (Supplementary Fig. 1b) which diverges to infinity at dc ($\omega = 0$). To be sensitive to LPCMO properties, we desire most of the ac current to flow through $R_2(\omega)$ and therefore choose frequencies to satisfy

$$R_2(\omega) = 1/\omega C_2(\omega) << R_0 = 10^{10}\Omega\ , \qquad \text{(S1)}$$

thereby determining a lower bound on ω.

The AH capacitance bridge reports the capacitance $C'(\omega)$ and the conductance $1/R(\omega)$ of the parallel equivalent circuit shown in Supplementary Fig. 1c. Using straightforward circuit analysis we relate the measured quantities $C'(\omega)$ and $R(\omega)$ to the circuit parameters of Supplementary Fig. 1b by the equations:

$$C'(\omega) = C_1(\omega)\left( \frac{R_2^2(\omega)}{(R_2(\omega)+R_s)^2 + \omega^2 R_2^2(\omega) R_s^2 C_1^2(\omega)} \right) , \qquad \text{(S2)}$$

and

$$R(\omega) = \frac{(R_2(\omega)+R_s)^2 + \omega^2 R_2^2(\omega) R_s^2 C_1^2(\omega)}{(R_2(\omega)+R_s) + \omega^2 R_2^2(\omega) R_s C_1^2(\omega)} \quad . \qquad \text{(S3)}$$

If $R_s$ is small enough to satisfy the relation

$$R_s << \min\left\{ \frac{1}{\omega C_1(\omega)}, \frac{1}{\omega C_2(\omega)}, \frac{1}{\omega C_1(\omega)}\left( \frac{C_2(\omega)}{C_1(\omega)} \right) \right\} \quad , \qquad \text{(S4)}$$

then equations S2 and S3 reduce respectively to $C'(\omega) = C_1(\omega)$ and $R(\omega) = R_2(\omega)$. Accordingly, the fulfillment of the constraints imposed by Eqs. S1 and S4 assures us that the ac dissipation is not due to leakage resistance and that the voltage drop across $R_s$ can be ignored. Under these conditions the measured complex capacitance has real, $C'(\omega)$, and imaginary, $C''(\omega) = 1/\omega R(\omega)$, parts that reflect respectively the polarization and the dissipation plotted and discussed in the Letter.

The constraints of Eqs. S1 and S4 now become

$$1/\omega C''(\omega) << R_0 = 10^{10}\,\Omega \qquad \text{(S5)}$$

$$R_s << \min\left\{ \frac{1}{\omega C'(\omega)}, \frac{1}{\omega C''(\omega)}, \frac{1}{\omega C'(\omega)}\left( \frac{C''(\omega)}{C'(\omega)} \right) \right\} \quad , \qquad \text{(S6)}$$

where we have replaced $C_1$ and $C_2$ by the measured quantities $C'$ and $C''$ respectively. These relations conveniently allow us to experimentally determine the range of frequencies over which $R_s$ can be safely ignored, thus guaranteeing that the equipotentials at ac are parallel to the film interface (Fig. 1c of Letter). We show in Supplementary Fig. 2 the $H = 0$ temperature dependence of the

impedance components, $1/\omega C'(\omega)$, $1/\omega C''(\omega)$ measured at 500 Hz and $R_{||}$ measured at dc. The corresponding temperature dependence of $C'(\omega)$ is shown in Fig. 1b of the Letter. Clearly the constraints of (S5) and (S6) are satisfied. It is not necessary to plot the third component of (S6) since $C''(\omega) > C'(\omega)$ for all of our data in the region of collapse (see Figs. 2-3 of Letter). We have verified that the constraints hold up to 20 kHz and at all the temperatures and fields used to

construct the phase diagram in Fig. 4 of the Letter. For our lowest frequency of measurement (100 Hz), we calculate $C''$ = 0.16 pF as a lower bound below which (S5) cannot be satisfied. For all of our data, $C''$(100 Hz) is more than a factor of ten higher and (S5) is thus satisfied for all of our low frequency data.

**Maxwell-Wagner analysis**

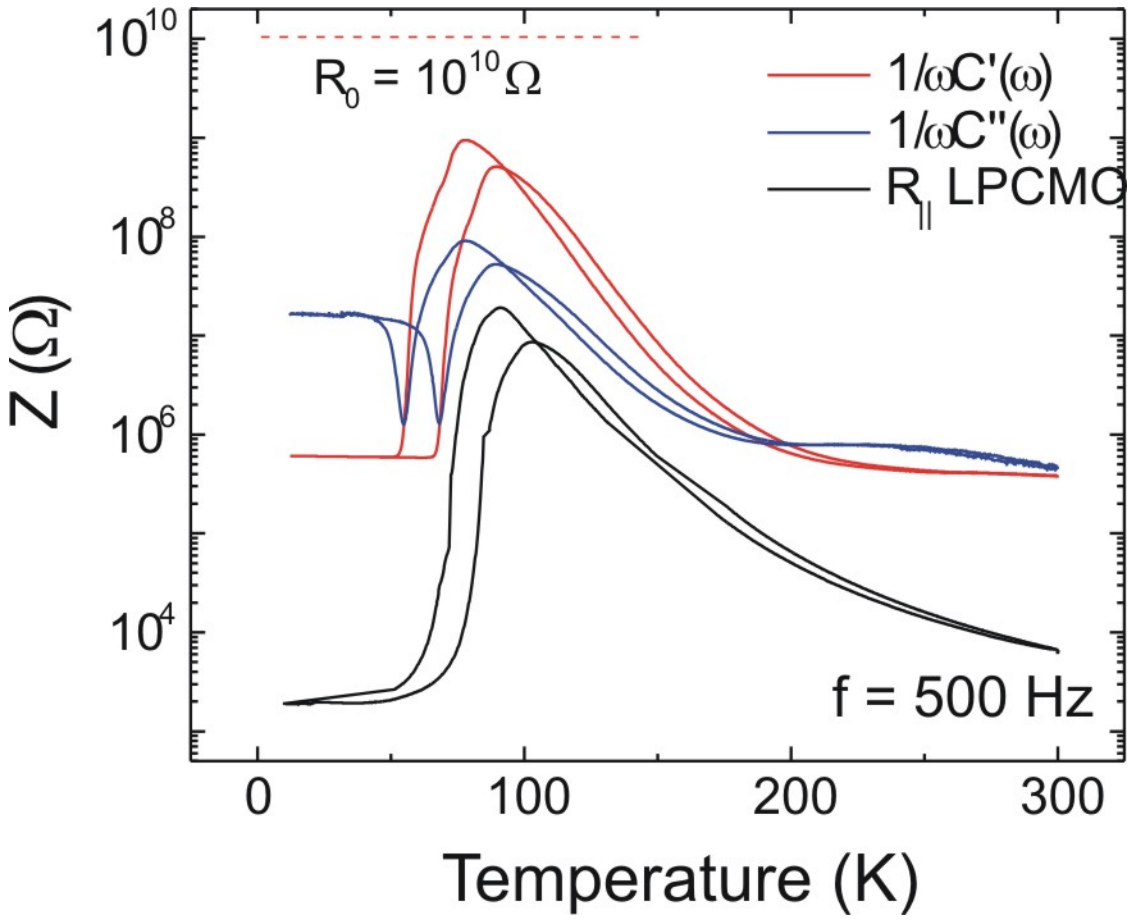


**Supplementary Figure 2 | Impedance plots verify that the longitudinal voltage drops are negligible compared to the perpendicular voltage drops:** The $H = 0$ temperature dependence of the impedance components $1/\omega C'(\omega)$, $1/\omega C''(\omega)$ measured at 500 Hz and $R_s = R_{||}$ measured at dc. The horizontal dashed line at $10^{10}\,\Omega$ represents the lower bound on $R_0$. Comparison of the relative magnitudes of these plots shows that at all temperatures the constraints imposed by Eqs. S5 and S6 are satisfied.

Having established the experimental conditions that allow us to ignore the series voltage drop across $R_s$,, we now must distinguish the dielectric responses of the manganite film and the AlOx capacitance. We model $C^*(\omega)$ using a Maxwell-Wagner (MW) circuit equivalent (Ref. 16 of Letter) in which impedance is represented as the series connection of two leaky capacitors. This configuration is often used to account for the effect of contacts in dielectric measurements. In our case the manganite impedance, expressed as a parallel combination of a resistance $R_M$ and capacitance $C_M$, is connected in series with a leak free capacitance $C_{AlOx}$ representing the Al/AlOx circuit element shown in Supplementary Fig. 1d. The resulting expression,

$$C^*(\omega) = C^*_{MW}(\omega) = \frac{C_{AlOx}}{1 + i\omega R_M C_{AlOx}/(1 + i\omega R_M C_M)}, \qquad \text{(S7)}$$

reveals a dielectric response determined by two time constants, $R_M C_{AlOx}$ and $R_M C_M$. As $\omega$ increases, the capacitance crosses over from being dominated by $C_{AlOx}$ to a capacitance dominated by the series combination of $C_{AlOx}$ and $C_M$ , i.e., $C^* = C_M C_{AlOx}/(C_M + C_{AlOx})$. If $C_M << C_{AlOx}$, as it is over much of the data range in Fig. 1b of the Letter and likewise for similar data taken in high magnetic fields, then C* in the 'high frequency' limit is equal to $C_M$ and is therefore a direct measure of the LPCMO dielectric response. We test these limits in Fig. 1b of the Letter by evaluating Re$\{C^*_{MW}(\omega)\}$ at 0.5kHz (green curve) using $C_M / C_{AlOx} = 10^{-4}$ and $R_M = R_{||}(T)^{\downarrow\uparrow}$ (black) as inputs. $C_M$ is assumed to be real for this calculation. The MW model thus provides a good qualitative account of the temperature-dependent capacitance (Fig 1b of Letter, green line) for $C_M$

independent of frequency and equal to $10^{-4}$ $C_{AlOx}$. The MW model also shows good alignment in temperature between the maximum in the resistance used as an input and the calculated capacitance minimum. Finally, we note that the large series-connected aluminum oxide capacitor serves as a reference capacitor, which by its presence 'decloaks' or makes visible the smaller manganite capacitance. If the frequency becomes too high, the constraint (S6) is violated and $R_s$ becomes visible, introducing longitudinal voltage drops that cannot be distinguished from the perpendicular drops.

In reality there is considerable dielectric loss, especially in the presence of magnetic field, and $C_M$ is frequency dependent and therefore complex. If we force $C_M$ in the MW calculation to be complex with, for example, a Debye response, the alignment between the resistance maximum and the capacitance minimum does not change. The Cole-Cole plots (Figs. 2 and 3 of the Letter) are the additional ingredients that clearly capture the interesting intrinsic dynamics of scale invariant dielectric response associated with the interplay of competing phases as discussed in the Letter.

It is worthwhile to further elaborate on intrinsic versus extrinsic effects. The MW model is usually used to ascertain the contributions of contacts and interfaces when the material of interest is sandwiched between two electrodes (Refs 4,5,7,17,18 of Letter). In capacitors with thick dielectrics, the interface region next to either electrode can have distinctly different properties than the interior bulk. Such a heterogeneous system is well described in the MW model by two series-connected leaky capacitors. If one of the leakage components, say

the interface, is magnetic field sensitive and exhibits magnetoresistance (MR), then the measured magnetocapacitance (MC) can be a consequence of the extrinsic properties of an interface contact rather than the intrinsic properties of the bulk. In the unconventional configuration described in the Letter, the interface contact is a dispersionless leak-free Al/AlOx capacitor as represented schematically in Fig. S1(d), and the observed MC is due to the intrinsic properties of the mixed phase LPCMO. Any interface effects between the AlOx and the LPCMO are negligible, since the factor of 1000 change in capacitance, which includes the region where power-law scaling collapse is observed, necessarily involves the entire manganite film as described in the concluding section of the Letter. In addition all extrinsic contributions from contacts to the LPCMO at the film edges (Fig 1a of Letter) are included in the resistance $R_s$, which as we have shown above, can be ignored when the frequency is chosen to satisfy the inequality of Eq. S6. Experimentally, this insensitivity was further checked by using silver paint or pressed indium for contacts as described in the Methods section of the Letter.

**Dependence of anisotropy on film thickness**

The insulator to metal (IM) transition in bulk LPCMO is due to a 3D percolation transition. However, as described in the Letter, the presence of strain at substrate/LPCMO interface gives rise to anisotropy as measured by two distinct IM transitions: one in the parallel direction, $T^{\downarrow\uparrow}_{IM,||}$, corresponding to resistance maxima, and the other in the perpendicular direction, $T^{\downarrow\uparrow}_{IM,\perp}$, corresponding to capacitance minima. To verify that the strain-induced

anisotropy decreases for thicker more bulk-like films, we have repeated the measurements at zero field for a set of films with three different thicknesses: *d* = 300Å, 600Å and 900Å.

Figure S3 shows the dependence of $T^{\downarrow\uparrow}_{IM,||}$ and $T^{\downarrow\uparrow}_{IM,\perp}$ on *d* for cooling

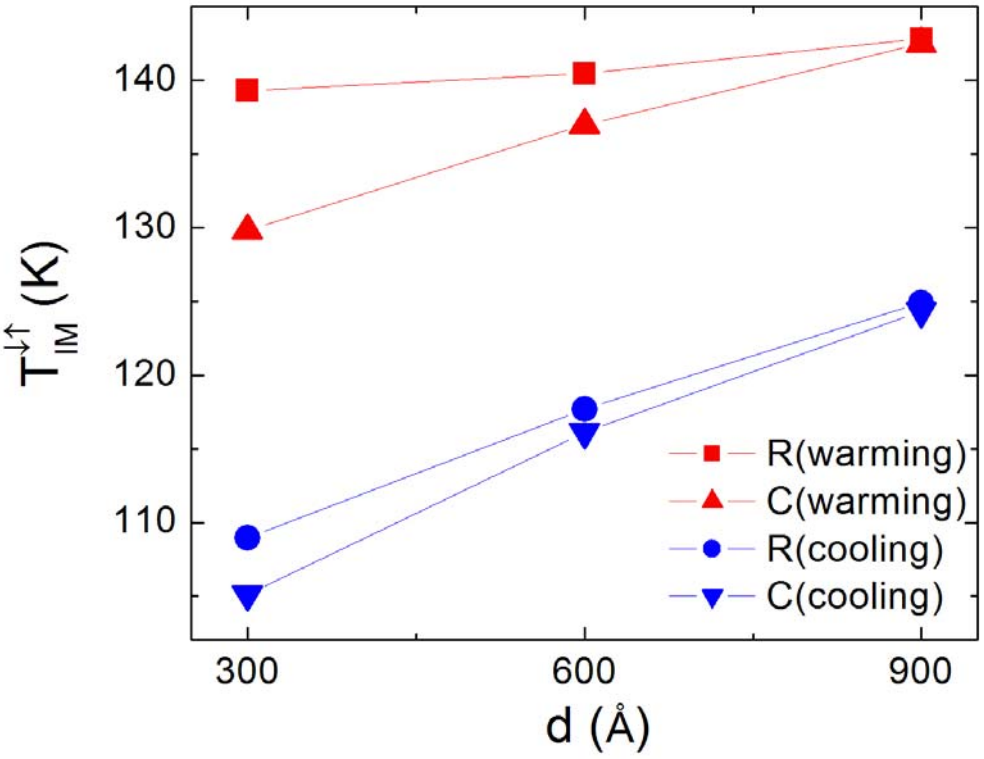


**Supplementary Figure 3 | With increasing LPCMO thickness *d* the anisotropic IM transitions move to higher temperatures:** The transition temperatures associated with resistance maxima (squares and circles) and capacitance minima (triangles) are identified in the legend and plotted as a function of *d* for cooling and warming. The capacitance data for the three different films are taken at 100 Hz and satisfy the impedance inequalities expressed in Eqs. S5 and S6 and shown in Fig. S2 for the 600 Å-thick sample described in the Letter.

and warming as labeled in the legend. For parallel transport the observed increase of transition temperatures can be qualitatively explained by the effect of dimensionality on percolation. Since percolation in 3D occurs at a lower metal fraction than it does in 2D, the IM transition increases with increasing *d* as is

indeed observed. This qualitative picture is complicated however by the presence of a strained layer at the substrate interface which contains a higher fraction of FMM phase. In this case conduction in the parallel direction is facilitated by the presence of the higher conductivity strained layer whereas in the perpendicular direction the current paths must thread regions containing a greater proportion of insulating phase, hence the difference between $T^{\downarrow\uparrow}_{IM,||}$ and $T^{\downarrow\uparrow}_{IM,\perp}$. The temperature differences, $\Delta T^{\downarrow\uparrow}_{IM} = T^{\downarrow\uparrow}_{IM,||} - T^{\downarrow\uparrow}_{IM,\perp}$, for cooling and warming are plotted versus *d* in Fig. S4. We note that the anisotropy does indeed decrease with increasing *d*. Thus as *d* increases the IM transition moves to higher temperature and transport becomes more isotropic as the effect of the strained interface diminishes.

The films discussed above were prepared from the same target but under different conditions than the 600 Å-thick film discussed in the Letter. The deposition conditions (oxygen pressure = 420 mTorr, substrate temperature = 820 °C, deposition rate = 0.5 Å/s) were determined by minimizing the transition width at an IM transition temperature ($T^{\downarrow}_{IM,||}$) that is close to the maximum value(cooling) observed in bulk compounds of the

same composition. The target was then conditioned with the same deposition parameters for many runs. In comparing the two 600 Å-thick films, we see that the transition temperatures $T^{\downarrow}_{IM,||}$ = 117.7K and $T^{\uparrow}_{IM,||}$ = 140.5K of the 'optimized' 600 Å-thick film shown in Fig. S3 are appreciably higher than the corresponding temperatures, $T^{\downarrow}_{IM,||}$=95K and $T^{\uparrow}_{IM,||}$=106K, of the film discussed in the Letter. In addition, the respective anisotropies for cooling ($\Delta T^{\downarrow}_{IM}$ = 1.5K) and warming

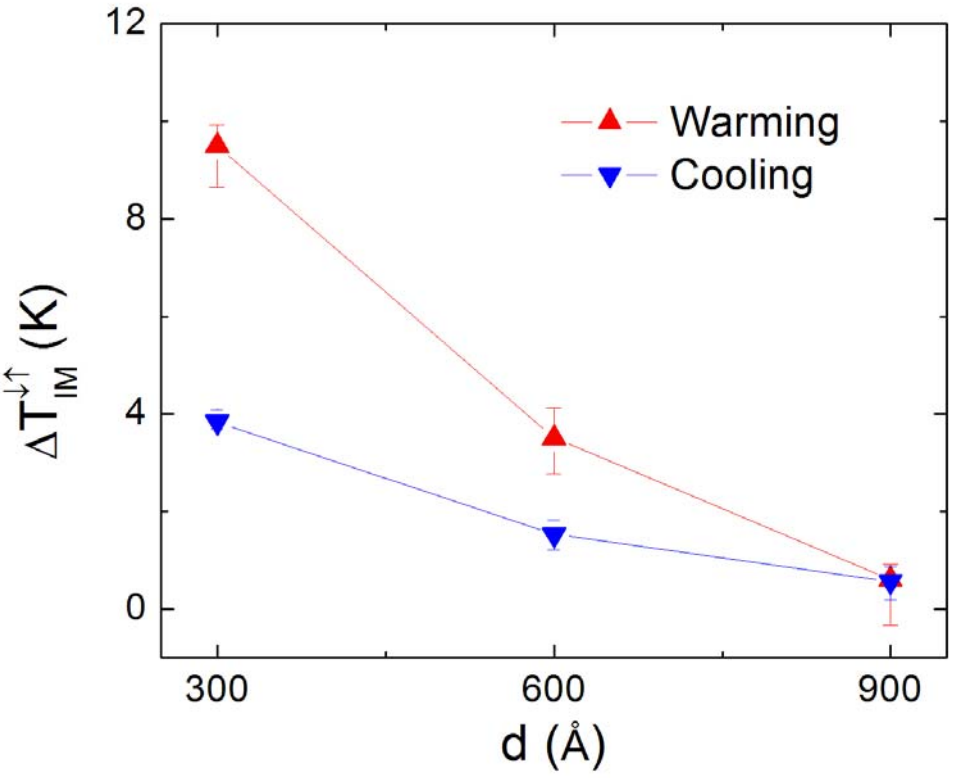


**Supplementary Figure 4 | With increasing LPCMO thickness the anisotropy as measured by $\Delta T^{\downarrow\uparrow}_{IM} = T^{\downarrow\uparrow}_{IM,||} - T^{\downarrow\uparrow}_{IM,\perp}$ decreases towards zero and bulk like behavior:** The data for both cooling and warming cycles at each thickness are obtained from the data shown in Fig. S3 by subtracting the temperature of the capacitance minimum (perpendicular transition) from the temperature of the resistance maximum. The error bars, which are on the order of the symbol size in Fig. S3, are determined by the temperatures which give a ±0.1% deviation at each extremum (resistance maximum or capacitance minimum).

($\Delta T^{\uparrow}_{IM}$ = 3.5K) of the 'optimized' 600 Å-thick film are significantly smaller than the corresponding anisotropies for cooling ($\Delta T^{\downarrow}_{IM}$ = 20K) and warming ($\Delta T^{\uparrow}_{IM}$ = 15K) of the same thickness film discussed in the Letter. These results show that our technique can advantageously be used to correlate anisotropies in LPCMO with deposition parameters. We anticipate that this capability will be applicable to other strongly-correlated complex oxide systems as well.